Prediction of Binary Gas Diffusion in Carbon Molecular Sieves at High Pressure

Huang Qinglin, S. Farooq, and I. A. Karimi
Dept. of Chemical & Environmental Engineering, National University of Singapore, Singapore 117576

A dual-resistance model, in which a barrier resistance confined at the micropore mouth is assumed to act in series with pore diffusional resistance distributed in the micropore interior, has been proposed for multicomponent transport of gases in carbon molecular sieves (CMS). Excellent predictive power of the model has been thoroughly validated by means of extensive unary/binary integral uptake and breakthrough measurements involving large pressure steps on Takeda and Bergbau Forschung (BF) CMS samples. Quantitative agreement between the experimental and predicted results is truly remarkable considering the fact that all the predictions are strictly based on independently measured single-component equilibrium and kinetic parameters. Impact of two mixture isotherms, namely ideal adsorbed solution (IAS) theory and extended Langmuir (E-L) model, on mixture uptakes has also been investigated. This study undeniably establishes the following: (1) effectiveness of a dual-resistance approach for gas transport in CMS micropores, and (2) much stronger concentration dependence of the transport parameters than that predicted from the use of a chemical potential gradient as the driving force for diffusion with constant intrinsic mobility. © 2004 American Institute of Chemical Engineers *AIChE J,* 50: 351–367, 2004
Keywords: carbon molecular sieves, adsorption/gas, diffusion (microporous)

Introduction

Many researchers have studied the transport mechanism of gases in carbon molecular sieve (CMS) micropores. Findings of several publications in this area are summarized in Table 1, where there seems to be no common agreement. Three different transport mechanisms have been identified. These are (1) pore model, in which the diffusional resistance is distributed in the micropore interior (Chagger et al., 1995; Chen et al., 1994; Liu and Ruthven, 1996; Rutherford and Do, 2000; Ruthven, 1992; Ruthven et al., 1986; Van Den Broeke and Krishna, 1995), (2) barrier model, in which the barrier resistance is confined at the micropore mouth (Dominguez et al., 1988; Fitch et al., 1994; LaCava et al., 1989; Liu and Ruthven, 1996; Reid and Thomas, 2001; Reid et al., 1998; Rynders et al., 1997; Srinivasan et al., 1995), and (3) dual resistance model (Liu and Ruthven, 1996; Loughlin et al., 1993; Reid and Thomas, 2001; Reid et al., 1998), which is a serial combination of barrier resistance at the micropore mouth followed by a distributed pore resistance in the interior. Nguyen and Do (2000) argued that adsorption in CMS could be divided into selective adsorption in micropores and nonselective adsorption in macropores and mesopores. A dual Langmuir kinetic model was proposed. It could explain the gas diffusion in Takeda 3A CMS well, but not the uptake data in Takeda 5A CMS.

The reported differences in mechanisms in the studies summarized in Table 1 cannot be linked to the manufacturer of the absorbent or the adsorbate gas. However, all the studies in which the concentration dependence of micropore diffusivity was explored seem to conform closely with the Darken's equation, which follows from the chemical potential gradient as the driving force for diffusion (Chihara et al., 1978; Kawazoe et al., 1974; Rutherford and Do, 2000; Ruthven, 1992)

$$\frac{D_c}{D_{co}} = \frac{d\ \ln c}{d\ \ln q} \tag{1}$$

where D_{co} is called the limiting diffusivity, which is the diffusivity in the Henry's law region of the isotherm (that is, fractional coverage, $\theta \rightarrow 0$). For a Langmuir isotherm

Correspondence concerning this article should be addressed to S. Farooq at chesf@nus.edu.sg.

Table 1. Summary of Important Publications on Transport Mechanism in CMS Micropores

Authors	Adsorbate	Adsorbent	Kinetic Model
Chagger et al. (1995)	$O_2/N_2/CO_2$	CMS	Pore diffusion
Chen et al. (1994)	O_2/N_2	BF CMS	Pore diffusion
Dominguez et al. (1988)	O_2/N_2	CMS	Barrier resistance
Fitch et al. (1994)	O_2/N_2	CMS	Barrier resistance
LaCava et al. (1989)	O_2/N_2	CMS	Barrier resistance
Liu and Ruthven (1996)	$O_2/N_2/Ar/CH_4/CO_2$	BF CMS	Pore diffusion: O_2, N_2, and Ar Barrier resistance: CH_4 Dual resistance: CO_2
Loughlin et al. (1993)	CH_4/N_2	BF CMS	Dual resistance
Nguyen and Do (2000)	$O_2/N_2/Ar$	Takeda CMS 3A	Dual Langmuir kinetic model
Reid and Thomas (2001)	$C_6H_6/CO/N_2/C_2H_2/C_2H_4/CH_4/CS_2$	CMS	Pore diffusion/barrier resistance/ dual resistance
Reid et al. (1998)	O_2/N_2/neon/Ar/Kr	CMS	Barrier resistance: O_2, N_2, Ar and Kr Dual resistance: neon
Rutherford and Do (2000)	CO_2	Takeda CMS 5A	Pore diffusion
Ruthven (1992)	O_2/N_2	BF CMS	Pore diffusion
Ruthven et al. (1986)	O_2/N_2	BF CMS	Pore diffusion
Rynders et al. (1997)	O_2/N_2	Takeda CMS	Barrier resistance
Srinivasan et al. (1995)	O_2/N_2	CMS	Barrier resistance
Van Den Broeke and Krishna (1995)	$CO_2/N_2/CH_4/C_3H_6/C_3H_8$	Takeda CMS 5A	Pore diffusion

$$\frac{D_c}{D_{co}} = \frac{1}{1-\theta} \tag{2}$$

One exception to the preceding is the study by Chen and Yang (1992), which used a kinetic theory approach to obtain

$$\frac{D_c}{D_{co}} = \frac{1}{1-(1-\lambda)\theta} \tag{3}$$

The reported values of λ for oxygen and nitrogen in a sample of Bergbau-Forschung (BF) CMS were 0.05282 and 0.01287, respectively (Chen et al., 1994). More recently, Wang et al. (2001) have reported that the concentration dependence of the diffusivity of carbon dioxide in a CMS membrane was much stronger than that predicted by Darken's equation.

Liu and Ruthven (1996) found that the barrier coefficient of carbon dioxide transport in BF CMS micropores depended on the adsorbent loading according to the following equation derived from the Langmuir kinetic model

$$\frac{k_b}{k_{bo}} = \frac{1}{1-\theta} \tag{4}$$

LaCava et al. (1989) had earlier shown that the Langmuir kinetics model was a good useful approximation of the more general slit potential rate model. Analogous to D_{co} in Eq. 1, k_{bo} is the limiting barrier coefficient, which is obtained from uptake measured in the linear range of the isotherm. Both D_{co} and k_{bo} have the usual exponential temperature dependence. The same form of concentration dependence of barrier coefficient may also be derived from the chemical potential gradient as the driving force for diffusion with adsorption equilibrium represented by the Langmuir isotherm (Srinivasan et al., 1995).

For a Langmuir isotherm, Eq. 4 may also be written as

$$\frac{k_b}{k_{bo}} = 1 + bc \tag{5}$$

where c is the adsorbate concentration in the gas phase and b is the Langmuir isotherm constant. A number of studies (Liu and Ruthven, 1996; Reid and Thomas, 2001; Rynders et al., 1997) have reported increasing barrier coefficients of oxygen and nitrogen in CMS with increasing sorbate partial pressures.

Among the studies mentioned earlier, only Chen et al. (1994) attempted to predict binary uptake from single-component information only. The partial pressure changes in most of their experimental runs were relatively small, and these were the runs that showed good agreement with the predictions. Only two runs involving significant changes in sorbate partial pressures were presented. For these two runs, the agreement was more qualitative than quantitative, particularly for the slower diffusing nitrogen.

From the preceding discussion, it is clear that in addition to the disagreement on the transport mechanism of gases in CMS micropores, there is also the lack of a proper model that gives reliable quantitative prediction of binary integral uptake in CMS adsorbents from single-component information.

In a recent study from this laboratory (Huang et al., 2003), adsorption and diffusion of oxygen, nitrogen, carbon dioxide, and methane were measured in a Takeda CMS sample (designated as Takeda I) over a wide range of pressure and temperature. Similar measurements were also made for oxygen and nitrogen in a BF CMS and a second Takeda CMS sample (designated as Takeda II). A dual-resistance model was shown to be the desirable unified approach that fitted the experimental results in the entire range covered in that study. As expected, both the transport parameters of the dual-resistance model were observed to be functions of the adsorbed phase concentration. However, surprisingly, the functions were significantly stronger than the Darken's equation (Eq. 2) and its equivalent equation for barrier coefficient (Eq. 4). In other words, the thermodynamically corrected transport parameters of the dual-resistance model were also strong functions of adsorbate concentration in the adsorbent. To account for the concentration dependence of the thermodynamically corrected transport parameters, an empirical but simple and effective procedure was proposed. The limiting, that is (thermodynamically corrected)

transport parameters, D_{co} and k_{bo}, have generally been found to be independent of θ in zeolite adsorbents where the pore size is uniform. In CMS adsorbents, since micropore sizes are distributed and the pore connectivities are not fully understood, it appeared logical to assign each pore size its own characteristic D_{co} and k_{bo} values. This argument, combined with the fact that pores are filled in the order of increasing size, requires D_{co} and k_{bo} to be increasing functions of θ. The following forms were validated for unary diffusion in our previous study (Huang et al., 2003)

$$D_{co} = D^*_{co}\left(1 + \beta_p \frac{\theta}{1-\theta}\right) \tag{6}$$

$$k_{bo} = k^*_{bo}\left(1 + \beta_b \frac{\theta}{1-\theta}\right) \tag{7}$$

where β_p and β_b were obtained by fitting experimental D_c/D^*_{co} vs. θ and k_b/k^*_{bo} vs. θ data, respectively. The terms D_c and k_b are related to D_{co} and k_{bo} by Eqs. 2 and 4, respectively. This model was experimentally verified with limited integral uptake data for oxygen and nitrogen in Takeda I CMS. It is important to note that D_c/D^*_{co} vs. θ and k_b/k^*_{bo} vs. θ data were obtained from differential uptake experiments, and no additional fitting parameter was used when the proposed empirical model was applied to predict integral uptake results.

In continuation of our previous study summarized earlier, the following advances are reported in this communication:

(1) Further verification of dual resistance with dynamic column experiments in the linear range.

(2) Additional verification of Eqs. 6 and 7 with more single-component integral uptake and column dynamics data.

(3) The following multicomponent extensions of Eqs. 6 and 7 and validation with binary integral uptake and column dynamics experiments

$$(D_{co})_i = (D^*_{co})_i\left(1 + \sum_{i=1}^{N} \beta_{pi} \frac{\theta_i}{1 - \sum_{j=1}^{N} \theta_j}\right) \tag{8}$$

$$(k_{bo})_i = (k^*_{bo})_i\left(1 + \sum_{i=1}^{N} \beta_{bi} \frac{\theta_i}{1 - \sum_{j=1}^{N} \theta_j}\right), \tag{9}$$

where $\theta_i = q_i/q_{si}$ and $i = 1, 2, \ldots, N$.

(4) Comparison of extended Langmuir (E-L) isotherm and ideal adsorbed solution (IAS) theory based on Langmuir isotherms regressed independently for each gas for predicting binary adsorption kinetics.

Experimental results for oxygen, nitrogen, and their mixtures on samples called BF CMS and Takeda I CMS in our previous communication (Huang et al., 2003) are used here. In the following sections, we will use Takeda CMS to mean Takeda I CMS.

Experimental

Measurement of single-component and binary integral uptakes

Differential Adsorption Bed Apparatus. A differential adsorption bed (DAB) was designed and fabricated in this laboratory to measure single-component and binary oxygen and nitrogen integral uptakes in BF and Takeda CMS samples at high pressures. The DAB measurement method was first used by Habgood (1958) and further developed and refined by Carlson and Dranoff (1987), Chen et al. (1994), and Do et al. (1991). It is a versatile method capable of providing simultaneous equilibrium and kinetic data for both single-component and multicomponent systems. Since a small amount of adsorbent is used, heat-transfer effects can be eliminated by using a high flow of gas. This method, however, is more time-consuming than a conventional batch uptake procedure. It needs a series of regeneration, adsorption, and desorption steps to get just one point of equilibrium or kinetic data. This setup is shown in Figure 1. For a detailed description, the readers are referred to a recently completed Ph.D. dissertation (Huang, 2002).

Experimental Procedure. Since the analysis of equilibrium and kinetic data from the DAB method requires the volume of the desorption system, V_d, the volume of the desorption bomb including the associated tubes was carefully measured and good accuracy was ensured by checking reproducibility a few times. In order to calibrate the TCD, known amounts of nitrogen, oxygen, and inert (helium) were mixed in the desorption bomb and passed to the gas chromatograph via the 6-port valve for analysis. The mole fractions were calculated from the pressure readings after introducing each type of gas. The integrated areas of the TCD responses were then plotted against the mole fractions. A linear relationship was observed experimentally in the range covered in this study.

The experimental procedure was similar for both single-component and binary integral uptake measurements. Premixed bottle gas was used for binary measurements. CMS samples were fully regenerated, then accurately weighed and placed in the respective adsorber. We used 0.98 g of BF CMS and 1.0 g of Takeda CMS. Densities of BF and Takeda CMS samples based on external volume (i.e., volume measured after sealing the pores) were 0.988 g/cc and 1.02 g/cc, respectively. Prior to each experimental run, the adsorber holding CMS particles was immersed in the silicon oil and heated to 200°C for 8 to 10 hr under high vacuum. During this procedure, the adsorber was also flushed intermittently with helium to ensure full regeneration. The desorption bomb was also purged with helium and evacuated several times to ensure that no residual adsorbate gas remained. Each experimental run involved seven steps, which are also detailed in the dissertation just mentioned (Huang, 2002).

Data Processing. The calculation of the adsorbed amount for every exposure is straightforward and unambiguous. Ideal gas law was assumed, since the final pressure in the desorption bomb was always in the 2–4-bar range. The following mass balance gives the number of moles adsorbed by the adsorbent:

$$n = \frac{(P_d y_d - P_b y_b) V_d}{R_g T} \tag{10}$$

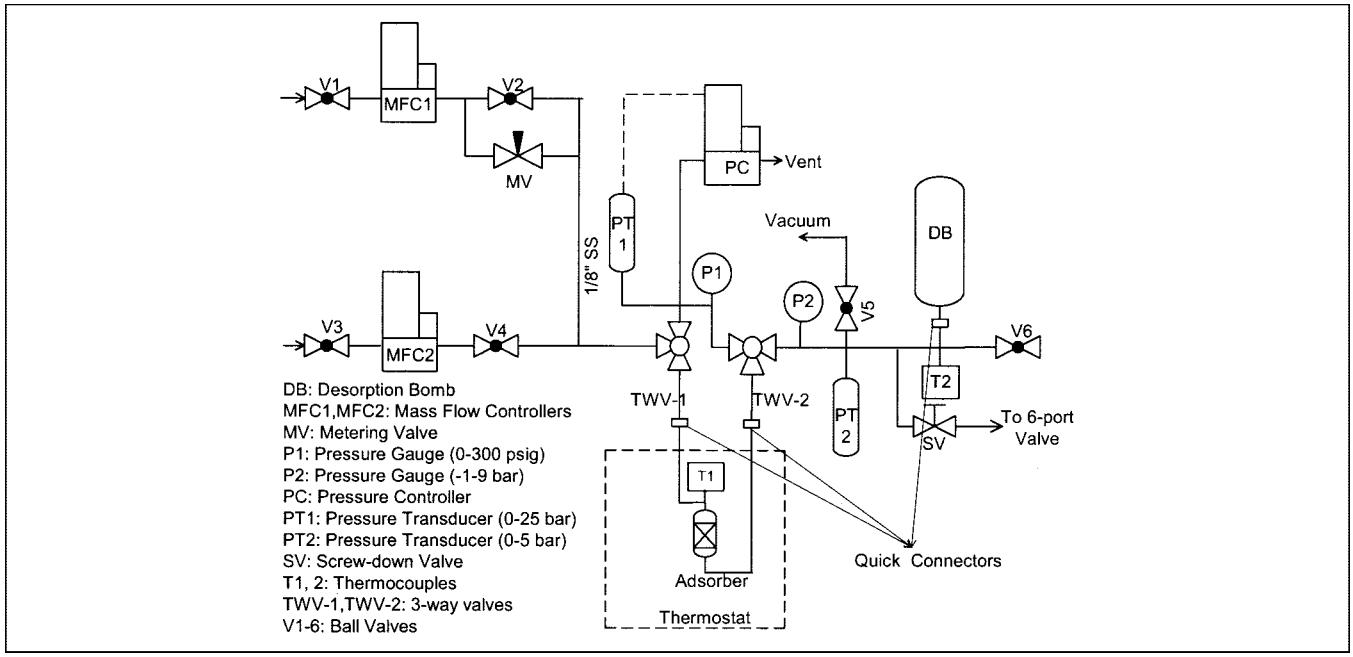

Figure 1. The differential adsorption bed (DAB) apparatus.

where P_d and P_b are the final pressures of the desorption bomb after integral uptake and blank measurements, respectively; y_d and y_b represent the corresponding mole fractions of the adsorbate gas; V_d is the volume of the desorption system; R_g is the gas constant; and T is the temperature of the desorption system. Temperature T was taken equal for two different measurements, because the stainless steel desorption bomb attained thermal equilibrium with the laboratory air (maintained at 19°C ± 1) when the pressure reading stabilized. The adsorbed amount based on macroparticle volume (q_{ip}) was then calculated from the weight and density of the adsorbent. Thus, the experimental fractional uptake equals the ratio q_{ip}/q^*_{ip}, where q^*_{ip} is the measured equilibrium adsorbed amount based on macroparticle volume.

Measurement of single-component and binary-column dynamics and binary equilibrium

A preexisting dynamic column breakthrough (DCBT) setup was modified in this study to measure single-component and binary-column dynamics as well as the binary equilibrium isotherm. A detailed description of the DCBT apparatus is given elsewhere (Malek, 1996; Malek and Farooq, 1996). The modification involved measuring flow at the exit of the adsorption column, which helped improve mass balance, and hence the accuracy of binary equilibrium data. More importantly, it provided an additional experimental observation to test the effectiveness of the proposed model for transport in CMS micropores. Single-component breakthrough curve in the linear range of the isotherm, as well as single-component and binary integral breakthrough curves corresponding to a step change in feed concentration were measured over a wide pressure range.

The column packed with CMS adsorbent particles was regenerated at 200°C for 10–12 hr with a continuous flow of helium. The packed column was then immersed in a liquid bath maintained at the desired temperature. The adsorption column and associated flow lines were further cleaned by flowing helium. The desired pressure level in the column was controlled by a back-pressure regulator. For the single-component runs, oxygen or nitrogen was fed by mixing with helium at a controlled rate. Feed concentration of the adsorbable component was varied by varying its proportion as well as the operating pressure. For the binary runs, either air or oxygen–nitrogen mixtures of other compositions were used. Adsorbate concentration and total flow rate were recorded at the exit. Oxygen concentration in the exit gas was continuously measured with an oxygen analyzer (Servomex, Model 572), while that of nitrogen was measured using a TCD. Constant readings of exit-gas concentration and flow rate were taken as the end of a breakthrough run. The change of gas flow rate along the column due to adsorption was negligible in low-concentration breakthrough measurements in the linear range of the isotherm. Hence, the exit flow rate was not measured in these runs.

For binary-exchange breakthrough measurements, the column was saturated with a known mixture of oxygen and nitrogen at a desired pressure. The saturated column was then purged with either pure oxygen or nitrogen until readings from the oxygen analyzer and exit flowmeter became constant again.

All the runs were corrected for dead volume by subtracting the blank response under identical operating condition. For more details on the blank correction, see Yuan (1997).

Binary Equilibrium Data from Breakthrough Response. In this study, binary isotherm data were measured from the binary exchange breakthrough experiments described earlier. Details of the experimental adsorption column, adsorbate, and adsorbent are listed in Table 2. The amount of the component displaced from the adsorbed phase during exchange was calculated in the same way as calculating a single-component isotherm from the single-component desorption breakthrough curve. The mean residence time of the desorption process was obtained from the following integral

Table 2. Column, Adsorbate, and Adsorbent Details for the Breakthrough Experiments

	Takeda CMS	BF CMS
Adsorption column	40 cm (length) × 3.8 cm (ID), stainless steel	40.2 cm (length) × 3.5 cm (ID), stainless steel
Bed voidage (ε_b)	0.35	0.29
Particle voidage (ε_P)	0.33*	0.33*
Particle radius (cm)	0.15	0.15
Particle density (gm/cc)	1.02	0.98
Adsorbate	O_2 (>99.8%); N_2 (>99.9%); Air; Helium (>99.99%)	O_2 (>99.8%); N_2 (>99.9%); Mixture gas (N_2:O_2 = 48:52); Helium (>99.99%)

*Assumed value.

$$\tau = \int_0^\infty \frac{v_e c_e}{v_o c_o}\, dt, \tag{11}$$

where v_o and v_e are the adsorbate inlet and outlet interstitial velocities; c_o ($=y_oP/R_gT$) and c_e ($=y_eP/R_gT$) are the adsorbate inlet and outlet concentrations, respectively; P is the system pressure; and y_o and y_e are the adsorbate inlet and outlet mole fractions, respectively.

Hence, the equilibrium adsorption capacity, q_p^*, corresponding to the partial pressure of the adsorbate in the feed could be derived from adsorbate material balance, giving the following equation upon rearrangement

$$q_p^* = \left(\frac{v_o\tau}{L} - 1\right)\frac{\varepsilon_b}{1-\varepsilon_b}\, c_o, \tag{12}$$

where L is the length of the packed column and ε_b is the bed voidage. Equilibrium adsorbed concentration per unit microparticle volume, q^*, was related to adsorbed concentration per unit macroparticle volume, q_p^*, by the following equation

$$q_p^* = (1-\varepsilon_p)q^* + \varepsilon_p c_o \tag{13}$$

In this equation, ε_p is the macropore voidage. In this study, macropore voidage of 0.33 was assumed for the two CMS samples.

Theoretical

Multicomponent equilibrium

Single-component oxygen and nitrogen isotherms in Takeda CMS and BF CMS measured by the constant-volume method were presented in the previous communication (Huang et al., 2003) along with fits of the Langmuir model. In that communication, the model was individually fitted to the oxygen and nitrogen data using the Langmuir model

$$q_i = \frac{q_{si} b_i c_i}{1 + b_i c_i} \tag{14}$$

This allowed oxygen and nitrogen to have different saturation capacities, q_{si}. An extension of the above model for the multicomponent system is the E-L isotherm given by

$$q_i = \frac{q_s b_i c_i}{1 + \sum_{i=1}^{N} b_i c_i}. \tag{15}$$

The above equation assumes that the saturation capacities of all gases are equal, that is, $q_{si} = q_s$. This assumption is required for the thermodynamic consistency of the E-L isotherm (Rao and Sircar, 1999), although strictly speaking, two gases cannot have identical q_s on any practical adsorbent. Thus, this assumption is usually made for the adsorption of molecules of comparable size, such as oxygen and nitrogen, with reasonable success (Farooq and Ruthven, 1991).

The Langmuir model, subjected to equal q_s, was used to reanalyze the data of Huang et al. (2003). The isotherm parameters and the corresponding residuals from the individual fits of Langmuir models and the collective fit of the Langmuir model subjected to equal q_s are compared in Table 3. Although the individual q_s values for nitrogen are ~17% and ~24% lower than those for oxygen on BF CMS and Takeda CMS, respectively, the residuals do not seem to suggest that the fit of data in the experimental range is significantly compromised by assuming equal q_s for the two gases.

An alternative to not forcing equal q_s is to use IAS theory for multicomponent prediction using individually fitted Langmuir models to represent the single-component isotherms. IAS the-

Table 3. Langmuir Isotherm Parameters for Oxygen and Nitrogen on BF CMS and Takeda CMS

		Different q_s for O_2 and N_2*				Same q_s for O_2 and N_2			
Adsorbent	Adsorbate	b_o** ($\times 10^{-3}$ cc/mmol)	$(-\Delta U)$** (kcal/mol)	q_s (mmol/cc)	Residual	b_o** ($\times 10^{-3}$ cc/mmol)	$(-\Delta U)$** (kcal/mol)	q_s (mmol/cc)	Residual
BF CMS	O_2	3.86	3.90	3.80	0.112	1.81	4.35	3.50	0.196
	N_2	2.80	4.26	2.87	0.058	4.08	3.83		0.301
Takeda CMS	O_2	3.48	3.98	4.34	0.064	3.79	3.96	3.96	0.156
	N_2	4.02	4.01	3.61	0.048	3.90	4.01		0.194

*From Huang et al. (2003).
**$b = b_o e^{-\Delta U/R_g T}$.

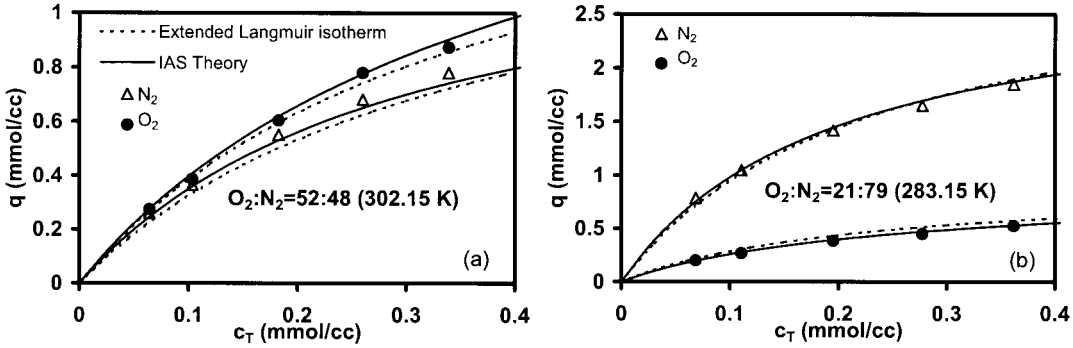

Figure 2. Binary isotherms for oxygen and nitrogen in (a) BF CMS and (b) Takeda CMS.

ory of Myers and Prausnitz (1965) is based on solution thermodynamics, and the basic thermodynamic equations for this theory are similar to those for vapor–liquid equilibrium. The equilibrium criterion states that the chemical potential for each component in the adsorbed phase is equal to that in the gas phase. Raoult's law is used to describe equilibrium for mixture adsorption

$$Py_i = P_i^o x_i \tag{16}$$

where x_i and y_i are the mole fractions of component i in the adsorbed phase and gas phase, respectively; P is the total pressure of the gas phase; P_i^o is the equilibrium gas-phase pressure corresponding to the adsorption of pure component i at the same spreading pressure, π, and the same temperature as for the adsorbed mixture. The Gibbs adsorption isotherm approach yields the spreading pressure π as follows

$$\frac{\pi A}{R_g T} = \int_0^{P_i^o} \frac{q_i}{P_i}\, dP_i \tag{17}$$

where A is the surface area per unit mass of adsorbent; P_i $(=Py_i)$ is the partial pressure of component i; and q_i is the measured adsorption isotherm of component i. In the present study, since the Langmuir model is used to represent single-component isotherm data, q_i in Eq. 17 can be replaced by the Langmuir model (Eq. 14) to get the following equation

$$\frac{\pi A}{R_g T} = \prod = q_{si} \ln\left(1 + \frac{b_i P_i^o}{R_g T}\right) \tag{18}$$

On the adsorbed surface, the mole fraction of gases must satisfy:

$$\sum_{i=1}^{N} x_i = 1 \tag{19}$$

Combining Eqs. 16, 18, and 19, we get

$$\sum_{i=1}^{N} \left(\frac{b_i P y_i}{R_g T(e^{\Pi/q_{si}} - 1)}\right) = 1 \tag{20}$$

where Π is the only unknown that can be solved by using the nonlinear equation solver subroutine NEQNF in IMSL. NEQNF uses a modified Powell hybrid algorithm and a finite difference approximation to calculate the Jacobian. After Π is known, we can get P_i^o from Eq. 18 and then x_i from Eq. 16.

From the fundamental definition of ideal adsorbed solution (Do, 1998)

$$\frac{1}{q_T} = \sum_{i=1}^{N} \frac{x_i}{q_i^o} \tag{21}$$

where q_T is the total adsorbed amount and q_i^o is the adsorbed amount of component i at pressure P_i^o, and follows the Langmuir isotherm

$$q_i^o = \frac{q_{si} b_i P_i^o / R_g T}{1 + b_i P_i^o / R_g T} \tag{22}$$

Therefore, the adsorbed amount for each component in a multicomponent mixture is obtained as

$$q_i = x_i q_T \tag{23}$$

The binary equilibrium predictions by the E-L model and IAS theory are compared with experimental results in Figure 2. It is clear that both the E-L model and IAS theory provide good prediction of the binary experimental equilibrium results. However, prediction by IAS theory appears to be somewhat superior quantitatively.

Column dynamics

Since the model for uptake in adsorbent particles in DAB experiments may be viewed as a limiting case of the model for an adsorption column in which the axial concentration gradient is negligible, we choose to present the equations for the more general case.

The following assumptions are made in order to develop the model for column dynamics:

(1) The flow pattern in the column is described by the axial-dispersed plug-flow model. Although the Peclet number in the adsorption column is usually high enough to approximate plug flow, the axial dispersion term is retained in the model

equations, since this facilitates numerical computation by eliminating discontinuities in the slope of the concentration profile.

(2) The ideal gas law applies and the system is isothermal.

(3) The frictional pressure drop through the column is negligible and the total column pressure is constant.

(4) The fluid phase and the adsorbent solid phase are linked through an external film resistance. The external film resistance is relatively small and may be neglected. This approach is often numerically more advantageous than the alternative approach of applying the equilibrium boundary condition at the solid surface.

(5) Molecular diffusion dominates in the macropores.

(6) Both macro- and microparticles are spherical.

(7) The transport behavior in the micropores is viewed as a series combination of barrier resistance confined at the micropore mouth followed by pore diffusional resistance in the interior of the micropores.

(8) The chemical potential gradient is the driving force for the diffusion across the micropore mouth and in the micropore interior.

(9) The limiting micropore transport parameters are increasing functions of adsorbent loading, as in Eqs. 8 and 9.

Subject to these assumptions, the equations given in Table 4 constitute the model for column dynamics.

Integral uptake

In view of the high flow of adsorbate gas and negligible thickness of the bed in DAB measurements, it is reasonable to assume a negligible concentration gradient between the inlet and outlet of the adsorber. Hence, Eqs. 31 to 40 given in Table 4 constitute the model equation for the uptake in DAB measurements with c_i related to the operating pressure of the system by the following equation

$$c_i = \frac{y_i P_{sys}}{R_g T_{sys}} \tag{41}$$

where P_{sys} and T_{sys} are the operating pressure and temperature of the differential adsorption bed; y_i is the mole fraction of component i in the feed.

The fractional uptake was calculated from volume integration of the concentration profiles in the macropores and micropores

$$\frac{q_{ip}}{q^*_{iP}} = \frac{\varepsilon_P \int_0^1 3c_{iP}\zeta^2 d\zeta + (1-\varepsilon_P)\int_0^1 3\bar{q}_i\zeta^2 d\zeta}{q^*_{iP}} \tag{42}$$

where

$$\bar{q}_i = \int_0^1 3q_i\eta^2 d\eta \tag{43}$$

and ζ $(=R/R_P)$ and η $(=r/r_c)$ are the dimensionless radial distances along the macroparticle and microparticle, respectively.

Model solution

The model equations were written in the dimensionless forms and then discretized in space by the method of orthogonal collocation. This reduced the coupled partial differential equations to a set of coupled algebraic (linear or nonlinear) and ordinary differential equations. For the prediction of column dynamics, the linear algebraic equations resulting from the overall mass balance were solved by Gaussian elimination to obtain velocity along the length of the column. The ordinary differential equations were integrated in the time domain using Gear's stiff variable-step integration routine provided in the FORSIM package to obtain composition of the gas and solid phase. For a binary system, the dual model for transport in micropores gives rise to the nonlinear boundary equations at $r = r_c$. These nonlinear equations and the nonlinear IAS theory equations were solved by using the nonlinear equation-solver subroutine NEQNF given in the IMSL package.

The number of collocation points is important in the accuracy of the numerical solution. The optimum numbers were determined by increasing collocation points until further change did not affect the solutions anymore. In the solutions of column dynamic models, 11 points for the external fluid field along the bed and 7 points each along the macroparticle or microparticle radii were used in all the simulations. In the solution of the uptake model, 16 collocation points along both the macroparticle and microparticle radii were used.

Results and Discussion

Unary system

Uptake in the Linear Range. The experimental uptake results of O_2 and N_2 in BF and Takeda CMS samples in the linear range ($\theta \rightarrow 0$) measured at more than three temperatures were analyzed with pore, barrier, and dual models. The best fits of these models to the experimental data were compared for a large number of cases in a recent publication from this laboratory (Huang et al., 2003). By referring to Figure 4 in that publication, it would be obvious even from a visual observation that in all the cases the best fit of the barrier model matched the early part of the experimental data well, but not the later part of the uptake. On the other hand, the solution of the pore model was distinctly different from the shape of the experimental uptake in the early part, but it fitted the later part of the data well. Undoubtedly, the dual-resistance model gave the best fit of the full range of uptake data in all the cases.

In order to optimize the fits of the three models (pore, barrier, and dual), a direct search was conducted by systematically varying the transport parameters in very small increments over a wide range. The minimum residuals for the three models are compared for a representative run in Figure 3. It is clear that the fit of the dual model is significantly superior to the fits of the pore and barrier models, which is indicated by the very small value of the minimum residual. The minimum residual for the dual-resistance model (0.0026) is an order of magnitude lower than that for the barrier model (0.043) and nearly two orders lower than the minimum value for the pore model (0.101). Such a comparison for the other runs gave similar results. The optimized transport parameters for the dual model are summarized in Table 5.

Some comments on the parameters reported in Table 5 are

Table 4. Model Equations for Calculating Dynamics of a Column Packed with CMS Adsorbent

External fluid phase material balance for component i:

$$\frac{\partial c_i}{\partial t} = D_L \frac{\partial^2 c_i}{\partial z^2} - v\frac{\partial c_i}{\partial z} - c_i\frac{\partial v}{\partial z} - \frac{1-\varepsilon_b}{\varepsilon_b}\frac{\partial q_{iP}}{\partial t}, \tag{24}$$

where D_L is the axial dispersion coefficient, which may be estimated by the following equation (Ruthven, 1984):

$$D_L = 0.7D_m + 0.5vd_p, \tag{25}$$

where d_p is the diameter of adsorbent particle, D_m is the molecular diffusivity, and v is the gas velocity; D_m may be calculatedfrom the Chapman-Enskog equation (Sherwood et al., 1975).

Continuity condition:

$$\sum_{i=1}^{n} c_i = c_T. \tag{26}$$

Overall mass balance:

$$\frac{\partial v}{\partial z} = -\frac{1-\varepsilon_b}{\varepsilon_b}\frac{1}{c_T}\sum_{i=1}^{n}\frac{\partial q_{iP}}{\partial t}. \tag{27}$$

Boundary conditions for the column:

$$D_L\left.\frac{\partial c_i}{\partial z}\right|_{z=0} = -v|_{z=0}(c_i|_{z=0^-} - c_i|_{z=0^+}); \qquad \left.\frac{\partial c_i}{\partial z}\right|_{z=L} = 0. \tag{28}$$

Velocity boundary conditions:

$$v|_{z=0^-} = v_o; \left.\frac{\partial v}{\partial z}\right|_{z=L} = 0. \tag{29}$$

The boundary condition at $z = L$ allows us to use the same collocation coefficients for the velocity profile as for the concentration profile in the fluid phase.

Mass transfer across external fluid film around adsorbent particle:

$$\frac{\partial q_{iP}}{\partial t} = \frac{3k_f}{R_p}(c_i - c_{ip}|_{R=R_p}) = \frac{3}{R_p}\varepsilon_p D_p\left.\frac{\partial c_{ip}}{\partial R}\right|_{R=R_P}. \tag{30}$$

Mass balance in macropore for component i:

$$\varepsilon_p\frac{\partial c_{ip}}{\partial t} + (1-\varepsilon_p)\frac{\partial \bar{q}_i}{\partial t} = \varepsilon_p D_p\left[\frac{\partial^2 c_{ip}}{\partial R^2} + \frac{2}{R}\frac{\partial c_{ip}}{\partial R}\right], \tag{31}$$

where $\bar{q}_i$ is the average adsorbed concentration of component i in the micropore.

Boundary conditions for the macropore balance:

$$\left.\frac{\partial c_{ip}}{\partial R}\right|_{R=0} = 0; \qquad {}_pD_p\left.\frac{\partial c_{ip}}{\partial R}\right|_{R=R_p} = k_f(c_i - c_{ip}|_{R=R_p}). \tag{32}$$

Mass balance at the micropore surface:

$$\frac{\partial \bar{q}_i}{\partial t} = -\frac{3}{r_c}J_i|_{r=r_c}. \tag{33}$$

The diffusion flux of component i to the microparticles in the preceding is derived from the chemical potential theory by introducing an imaginary gas phase concentration (Hu and Do, 1993):

$$J_i = -(D_{co})_i\frac{q_i}{c_i^{im}}\frac{\partial c_i^{im}}{\partial r}, \tag{34}$$

where c_i^{im} is an imaginary gas-phase concentration in equilibrium with the adsorbed phase concentration. It is imaginary because there is no gas inside the microparticle.

Mass balance in the micropores:

$$\frac{\partial q_i}{\partial t} = \frac{1}{r^2}\frac{\partial}{\partial r}\left\{r^2\left((D_{co})_i\frac{q_i}{c_i^{im}}\frac{\partial c_i^{im}}{\partial r}\right)\right\}. \tag{35}$$

Boundary conditions for the microparticle balance:

$$\left.\frac{\partial c_i^{im}}{\partial r}\right|_{r=0} = 0; \frac{3(D_{co})_i}{r_c}\left.\frac{\partial c_i^{im}}{\partial r}\right|_{r=r_c} = (k_{bo})_i\frac{\partial c_i^{im}}{\partial q_i}(q_i^* - q_i)|_{r=r_c}. \tag{36}$$

In Eqs. 35 and 36, $(D_{co})_i$ and $(k_{bo})_i$ are given by Eqs. 8 and 9, respectively.

For a single-component system, linear isotherm was used for measurements in the linear range and Langmuir isotherm for the integral runs. Accordingly, c_i^{im}, $\partial c_i^{im}/\partial q_i$, and q_i^* were calculated using:

$$c_i^{im} = \frac{\theta_i}{b_i(1-\theta_i)}; \qquad \frac{\partial c_i^{im}}{\partial q_i} = \frac{1}{K_{ci}(1-\theta_i)^2}; \qquad q_i^* = \frac{K_{ci}c_{ip}}{1+b_ic_{ip}}, \tag{37}$$

which reduce to

$$c_i^{im} = \frac{q_i}{K_{ci}}, \qquad \frac{\partial c_i^{im}}{\partial q_i} = \frac{1}{K_{ci}}$$

and $q_i^* = K_{ci}c_{ip}$ for a linear isotherm.

When the E-L isotherm was used for a binary system, the imaginary gas-phase concentrations were obtained by

$$c_A^{im} = \frac{\theta_A}{b_A(1-\theta_A-\theta_B)}; \qquad c_B^{im} = \frac{\theta_B}{b_B(1-\theta_A-\theta_B)}. \tag{38}$$

Using Eq. 38, the boundary conditions (Eq. 36) at $r = r_c$ become:

$$\left.\begin{aligned}\frac{3(D_{co})_A}{r_c}\left.\frac{\partial c_A^{im}}{\partial r}\right|_{r=r_c} &= \frac{(k_{bo})_A}{b_A(1-\theta_A-\theta_B)^2}[(1-\theta_B)(\theta_A^*-\theta_A) + \theta_A(\theta_B^*-\theta_B)]|_{r=r_c}\\ \frac{3(D_{co})_B}{r_c}\left.\frac{\partial c_B^{im}}{\partial r}\right|_{r=r_c} &= \frac{(k_{bo})_B}{b_B(1-\theta_A-\theta_B)^2}[\theta_B(\theta_A^*-\theta_A) + (1-\theta_A)(\theta_B^*-\theta_B)]|_{r=r_c}\end{aligned}\right\}, \tag{39}$$

where

$$\theta_A^* = \frac{b_Ac_{Ap}}{1+b_Ac_{Ap}+b_Bc_{Bp}}; \qquad \theta_B^* = \frac{b_Bc_{Bp}}{1+b_Ac_{Ap}+b_Bc_{Bp}}. \tag{40}$$

When employing IAS theory for binary equilibrium, the imaginary gas-phase concentrations, c_A^{im} $(=Py_A/R_gT)$ and c_B^{im} $(=Py_B/R_gT)$ were obtained from Eq. 16, and equilibrium adsorbed amounts, q_A^* and q_B^*, were obtained from Eq. 23. The sequence of calculations for IAS theory was discussed in the previous section. The derivation of boundary conditions at $r = r_c$ in Eq. 36 for IAS theory is somewhat tedious and is detailed in the Appendix.

Note that the barrier and pore models are two extremes of the dual model. The dual model solution reduces to that of the barrier model when a large value is assigned to the micropore diffusivity, and vice versa.

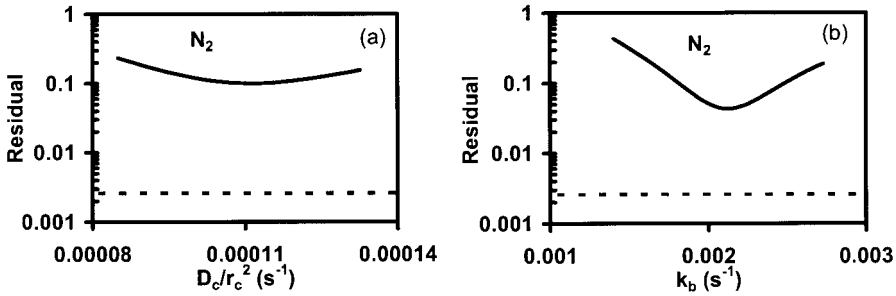

Figure 3. Comparison of the minimum residual obtained by optimizing the fits of (a) pore model and (b) barrier model for a representative uptake experiment in Takeda CMS: the dotted lines represent the minimum residual (=0.0026) of the dual model fit.

perhaps in order here. Loughlin et al. (1993) have reported the transport coefficients determined from a dual-micropore resistance model for the diffusion of methane and nitrogen in the micropores of BF CMS. Their nitrogen values ($D^*_{co}/r_c^2 = 0.227 \times 10^{-3}$ s^{-1}, $k^*_{bo} = 1.63 \times 10^{-2}$ s^{-1} at 323 K) are of comparable magnitude with our nitrogen data. The transport coefficient values for oxygen and nitrogen in CMS micropores reported in other studies are from the fit of either the pore diffusion model (Chen et al., 1994; Ruthven, 1992; Ruthven et al., 1986) or the barrier resistance model (Reid et al., 1998; Reid and Thomas, 1999; Rynders et al., 1997). Representative values in the literature have been compiled by Rynders et al. (1997). Transport coefficients determined in these studies most likely represent the combined effect of two resistances. Hence, as expected, these values are consistently lower than our values obtained from a dual model.

The observed difference in adsorption kinetics between nitrogen and oxygen is experimentally well established in the literature and it is attributed to the fact that the former has a fraction of an angstrom larger kinetic diameter than the latter. Higher activation energy for nitrogen (compared to oxygen) also draws support from other experimental studies (Ruthven, 1992; Reid et al., 1998). Nguygen and Do (2000) have shown from a potential field calculation between graphite layers in a CMS (i.e., in the slit-shaped micropores) that higher activation energy for nitrogen also results from the small difference in kinetic diameter. It also has been shown that the difference in activation energy between the two gases increases with reducing pore width.

Breakthrough in the Linear Range. In order to further confirm the gas transport behaviour in CMS micropores, breakthroughs of oxygen and nitrogen in an initially clean CMS bed were measured for low adsorbate concentrations (<5%) at nearly atmospheric pressure to remain within the linear range of the isotherm. Operating details of these experiments are given in Table 6. The optimum transport parameters for the three models obtained from the volumetric uptake measurements discussed in the previous section were directly applied to predict these experiments.

Representative comparisons between the predicted and measured data are shown in Figure 4 along with the residuals between experimental results and model predictions. The inadequacy of the pore model for the nitrogen runs (1 and 3) in both BF and Takeda CMS is evident from visual inspection and quantitatively supported by the relatively high residuals. The prediction by the dual model is undoubtedly the best for nitrogen breakthrough in Takeda CMS (Run 3). Although the residuals for the barrier model and the dual model are comparable in the case of nitrogen breakthrough in BF CMS (Run 1), the overall trend is better predicted by the latter. The magnified inset illustrates the more accurate prediction by the dual model in the range $c_{N_2}/c_o > 0.9$. The three predictions are quite comparable for oxygen breakthrough in both of the adsorbents. This is, in fact, consistent with our previous observation that it is not easy to reach experimental conditions at which the mechanism of oxygen transport in CMS micropores can be distinguished by means of breakthrough results (Farooq et al., 2002). Nevertheless, the results in Figure 4 do endorse that

Table 5. Transport Parameters of Oxygen and Nitrogen for the Dual Model in BF CMS and Takeda CMS

Adsorbent	Adsorbate	Temp. (K)	D^*_{co}/r_c^2 ($\times 10^{-3}$ s^{-1})	D'_{co}/r_c^{2**} (s^{-1})	E_d** kcal/mol	β_p†	β_p††	k^*_{bo} ($\times 10^{-2}$ s^{-1})	k'_{bo}** (s^{-1})	E_b** kcal/mol	β_b†	β_b††
BF CMS	O_2	302.15	6.84	5.70	4.01	0	0	24	919.38	5.01	5.56	3.95
		267.65	3.27					7.57				
		253.15	1.85					4.57				
	N_2	302.15	0.43	83.94	7.32	0.61	1.44	1.06	121.61	5.62	2.07	4.01
		283.15	0.18					0.51				
		275.15	0.13					0.44				
Takeda CMS	O_2	267.65	4.78	55.63	4.98	0	0	8.1	2862.4	5.57	5.56	3.95
		253.15	2.80					4.45				
	N_2	302.15	0.58	706.31	8.42	0.61	1.44	0.88	819.83	6.88	2.07	4.01
		283.15	0.22					0.39				
		273.15	0.13					0.26				

**$D^*_{co}/r_c^2 = (D'_{co}/r_c^2)e^{-E_d/R_gT}$; $k^*_{bo} = k'_{bo}e^{-E_b/R_gT}$.
†Based on unconstrained Langmuir model fit.
††Based on Langmuir model fit by constraining equal q_s.

Table 6. Operating Details of Single Component and Binary Breakthrough Experiments*

Run No.	Adsorbent	Pressure, P (bar)	Initial Condition	Feed	Interstitial Inlet Velocity, v_o (cm/s)	Temp., T (K)
1	BF CMS	1.4	Purged with helium	2.9% N_2	0.96	283.15
2				3.1% O_2	4.81	
3	Takeda CMS	1.4		2.9% N_2	1.92	
4		1.2		3.0% O_2	4.81	
5		8		40.6% N_2	0.93	274.15
6	BF CMS	8		50.8% N_2	0.93	
7	Takeda CMS	8.5	Saturated with N_2: O_2 = 79:21	O_2	0.98	
8	BF CMS		Saturated with N_2: O_2 = 48:52			
9	Takeda CMS		Saturated with N_2: O_2 = 79:21	N_2		
10	BF CMS		Saturated with N_2: O_2 = 48:52			

*Common parameters are given in Table 2.

only the dual model can capture the transport behavior of both oxygen and nitrogen in the two CMS samples. Such a unified model is essential for the prediction in multicomponent systems.

Hence, in the following sections, only the dual model will be verified further by comparing its prediction with the data from single-component and binary integral-uptake and column-dynamics measurements. Two versions of the dual model will be investigated. The dual model with $\beta_{iP} = \beta_{ib} = 0$ will be referred to as Dual Model 1, while that with β_{iP} and β_{ib} from Table 5 will be called Dual Model 2. It should be emphasized that Dual Model 1 assumes chemical potential gradient as the driving force for diffusion with constant (pore-size independent) limiting transport parameters. On the other hand, according to Eqs. 8 and 9, Dual Model 2 allows for pore-size dependence of the limiting transport parameters. In the case of binary systems, there will be a further subdivision based on the isotherm model used for binary equilibrium prediction, namely E-L isotherm and IAS theory.

It should be emphasized that the model predictions for all the comparisons presented in the following sections were calculated by directly applying the independently measured equilibrium and kinetic parameters compiled in Tables 3 and 5 without any kind of tuning or adjustment. How these parameters were estimated is discussed under the respective sections. It would perhaps be useful to review the highlights before discussing predictions of unary/binary integral uptake and breakthrough results.

The equilibrium parameters are b_i and q_{si}, which were obtained by fitting the Langmuir model to experimental unary equilibrium data (see under "Multicomponent Equilibrium"). The kinetic parameters related to diffusion in the micropores are $(D^*_{co}/r_c^2)_i$, $(k^*_{bo})_i$, β_{pi} and β_{bi}. D_p $(=D_m/\tau)$, is the only input parameter for macropore diffusion. Molecular diffusivity, D_m, was estimated from the Chapman Enskog equation (Sherwood et al., 1975), while a typical value of 3 was used for tortuosity factor, τ (Malek and Farooq, 1997). $(D^*_{co}/r_c^2)_i$ and $(k^*_{bo})_i$ were obtained by optimizing the fit of the dual-micropore resistance model to unary uptake data in the linear range of the isotherm (i.e., at very low coverage), as discussed in a previous section (see "Uptake in the Linear Range"). Unary diffusional uptake measured over a wide range of adsorbent loading gave D_c/D^*_{co} vs. Θ and k_b/k^*_{bo} vs. data, which were fitted, respectively, to Eqs. 2 and 6 to obtain β_p, and to Eqs. 4 and 7 to obtain β_b (Huang et al., 2003).

Table 7. Parameters for the Pore and Barrier Models

Adsorbent	Adsorbate	Pore Model D^*_{co}/r_c^2 ($\times 10^{-3}$ s^{-1})	Barrier Model k^*_{bo} ($\times 10^{-2}$ s^{-1})
BF CMS	O_2	2.70	4.96
	N_2	0.10	0.25
Takeda CMS	O_2	4.20	6.90
	N_2	0.12	0.21

Axial dispersion, D_L, and external film mass-transfer coefficient, k_f, are the two other additional transport parameters necessary to predict column dynamics. Here, D_L was estimated from Eq. 25 and k_f was calculated from the following correlation given by Wakao and Funazkri (1978): $Sh = 2.0 + 1.1Sc^{1/3}Re^{0.6}$.

Integral Uptake. The integral uptakes of oxygen and nitrogen in BF and Takeda CMS were measured for a step change in pressure from 0 to 10 bar at two different temperatures. The model predictions are compared with some representative experimental results in Figure 5.

In both the CMS samples, Dual Model 1 seems to capture the trends of experimental results qualitatively, but the quantitative departure is large. Except for some deviation in the early part of nitrogen uptake in BF CMS, Dual Model 2 provides an excellent prediction of the experimental results. The observed difference for nitrogen uptake in BF CMS is consistent with that seen for the corresponding breakthrough result in the linear range (see Run 1 in Figure 4). It appears that the contribution of the limiting barrier resistance might have been underestimated from the differential uptake measurements in the linear range. Indeed, the difference could be improved by making a small adjustment to k_{bo}. Overall, however, it is clear that the stronger concentration dependence of the transport parameters has a large impact on the uptakes, and the proposed empirical equations successfully account for the observed behaviour.

Integral Breakthrough. In these experiments, feed streams at 8 bar containing 40–50% nitrogen in helium were introduced to fully regenerated CMS beds. The operating details of these

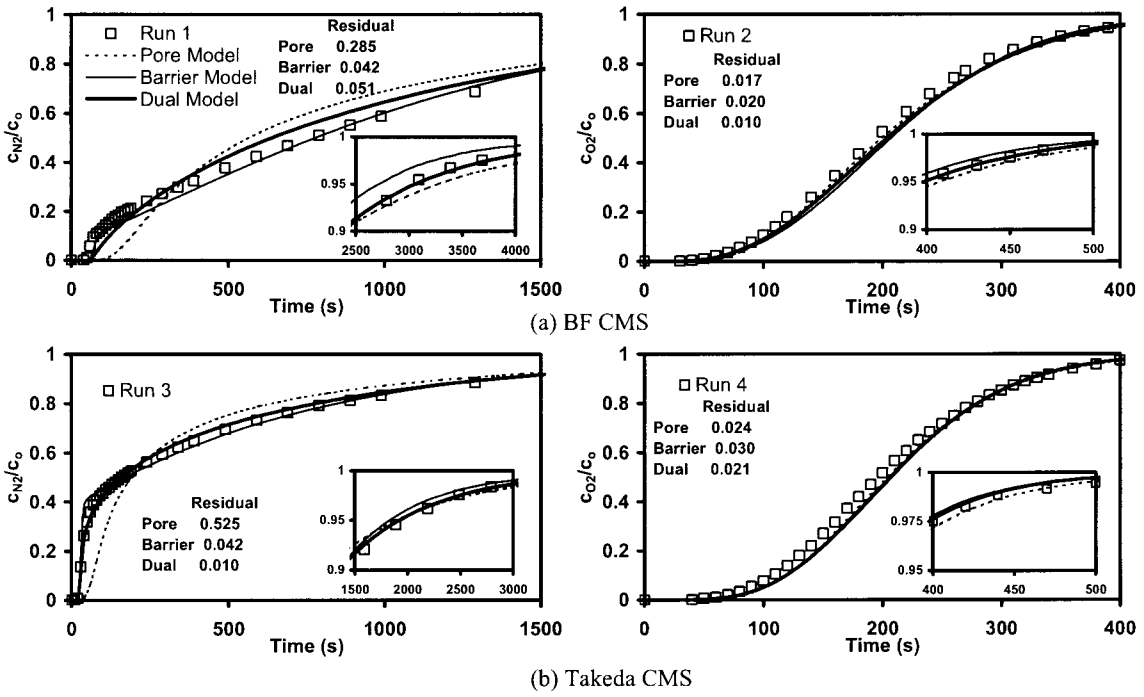

Figure 4. Low concentration breakthrough of oxygen and nitrogen in (a) BF CMS and (b) Takeda CMS are compared with prediction of the three models.

Experimental details are given in Table 6. The transport parameters used to simulate these runs are directly taken from the optimum fits of the three models to the uptake data. The dual model parameters are given in Table 5. The parameters for the pore and the barrier models are tabulated in Table 7.

runs are given in Table 6. The column response to a step change at the inlet was continuously monitored at the exit. Both nitrogen concentration and the flow rate of the exit stream were measured.

The experimental results together with the dual model predictions are shown in Figure 6. As mentioned earlier, the exit velocity profile was an additional measured variable to verify the effectiveness of the proposed theoretical model. The impact

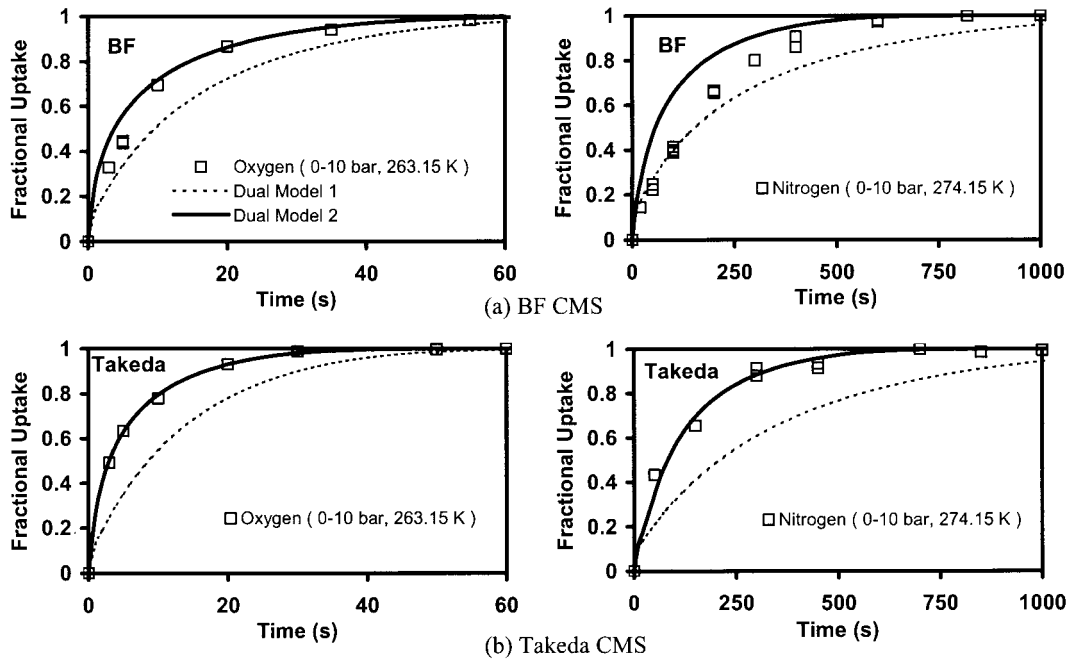

Figure 5. Single-component integral uptakes of oxygen and nitrogen in (a) BF CMS, and (b) Takeda CMS and model predictions.

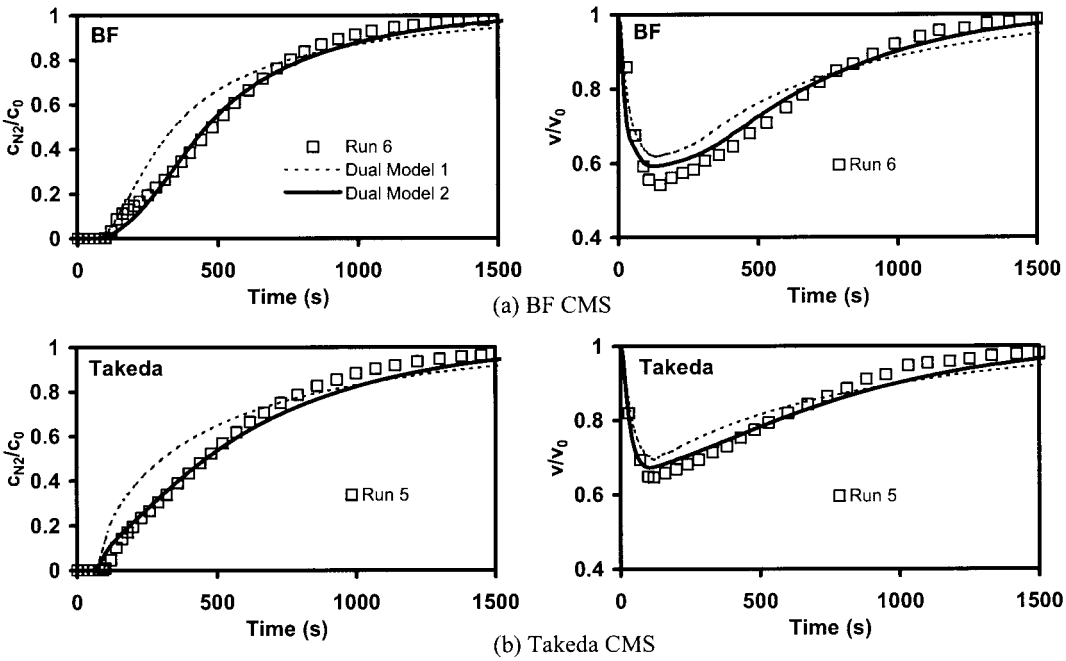

Figure 6. Exit concentration and velocity breakthrough profiles of nitrogen at high feed concentration measured in an initially clean (a) BF CMS and (b) Takeda CMS bed are compared with model predictions.

See Table 6 for experimental details.

of the stronger concentration dependence of the two transport parameters is observed in both the profiles. Dual Model 2 correctly captures the observed trends and provides very good quantitative agreements, while Dual Model 1 is clearly inadequate.

Binary system

Integral Uptake. In order to verify the proposed multicomponent extensions of the empirical equations (Eqs. 8 and 9), binary codiffusional uptakes of a 50:50 oxygen–nitrogen mixture in BF and Takeda CMS samples were measured for a step change of 0 to 10 bar. Representative comparisons between the experimental results and model predictions are shown in Figure 7. Here both the E-L model and IAS theory were used for binary equilibrium calculations with parameters from Table 3. The β values for the Langmuir model by constraining equal q_s are listed in Table 5, together with those for the individual Langmuir model.

The stronger concentration dependence of the transport parameters is clearly evident in the binary uptakes of both the gases. The abilities of these extended empirical models to capture the stronger concentration dependence, and the quantitative agreements achieved with no additional tuning parameters are quite remarkable. The difference between the predictions of the E-L model and IAS theory is indeed small. However, like the marginally better prediction of binary equilibrium data by the IAS theory, the prediction of Dual Model 2 with IAS theory also appears to show a small but visible improvement in most cases.

The roll-up in oxygen uptake is predicted by both Dual Models 1 and 2. Oxygen diffuses into micropores faster than nitrogen. More oxygen than its binary equilibrium value is adsorbed initially, which manifests as the roll-up after being replaced by the slower diffusing nitrogen. The location and extent of roll-up depend on the difference in kinetics of the two species, and in this regard, Dual Model 2 is clearly superior. Dual Model 2 slightly overpredicts the early part of oxygen uptake, but provides good prediction in the later long tailing part. As can be seen from Figure 7, at the peak of roll-up, the fractional uptake of nitrogen is only about 0.3. Therefore, most of the gas in the micropores must have been oxygen and its uptake had very little influence from nitrogen. Nitrogen slowly diffuses into the micropores and replaces oxygen. The long oxygen tail therefore represents binary exchange controlled by nitrogen uptake. That is why the impact of the stronger concentration dependence of the transport parameters is also evident even in the tailing part.

Integral Breakthrough. Having verified Eqs. 8 and 9 with binary uptakes measured at the particle scale, these equations were implemented for the breakthrough simulation and verified with binary integral breakthrough experiments conducted with both the adsorbents. In these experiments, the adsorption column was initially saturated with a mixture of oxygen and nitrogen and then purged with either oxygen or nitrogen at the same pressure. The conditions of these counterdiffusion experiments are summarized in Table 6.

The experimental runs and model predictions are compared in Figures 8 and 9. Stronger concentration dependence of the transport parameters is evident in all cases. Moreover, it is also clear that the extended empirical approach is equally effective in capturing the impact on column dynamics. Dual Model 1 is unable to predict even the right shapes of concentration breakthrough results and exit velocity profiles.

The quantitative improvement due to the use of IAS theory as compared to the E-L model is somewhat more obvious for the breakthrough experiments than it was in the case of the

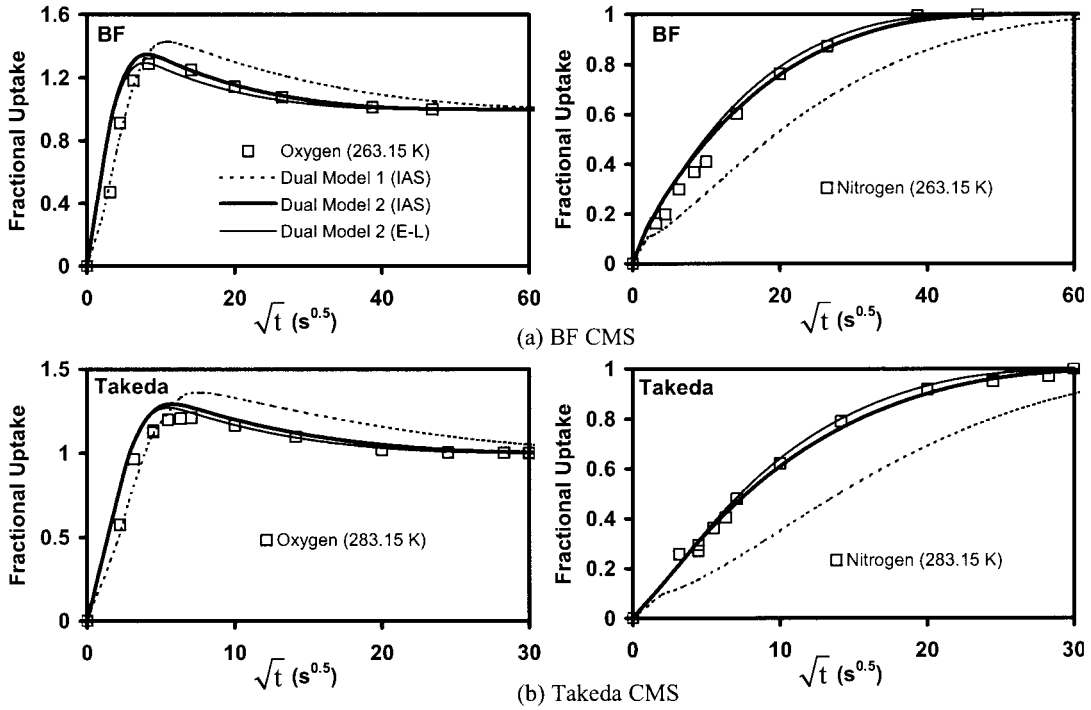

Figure 7. Prediction of binary integral uptakes of oxygen and nitrogen in (a) BF CMS and (b) Takeda CMS.

Pressure step: 0–10 bar.

uptake runs. Exit velocity profiles predicted by Dual Model 2 with IAS theory are in excellent agreement with those measured for all four cases in Figures 8 and 9. The same also holds for the concentration breakthrough of nitrogen purge in beds saturated with a oxygen–nitrogen mixture (Figure 9). For oxygen purge, the predicted concentration profiles are practically unaffected by the two isotherm models.

Unlike the excellent agreement in other cases, there is some difference between the measured breakthrough of the oxygen purge in a BF CMS bed saturated with a oxygen–nitrogen

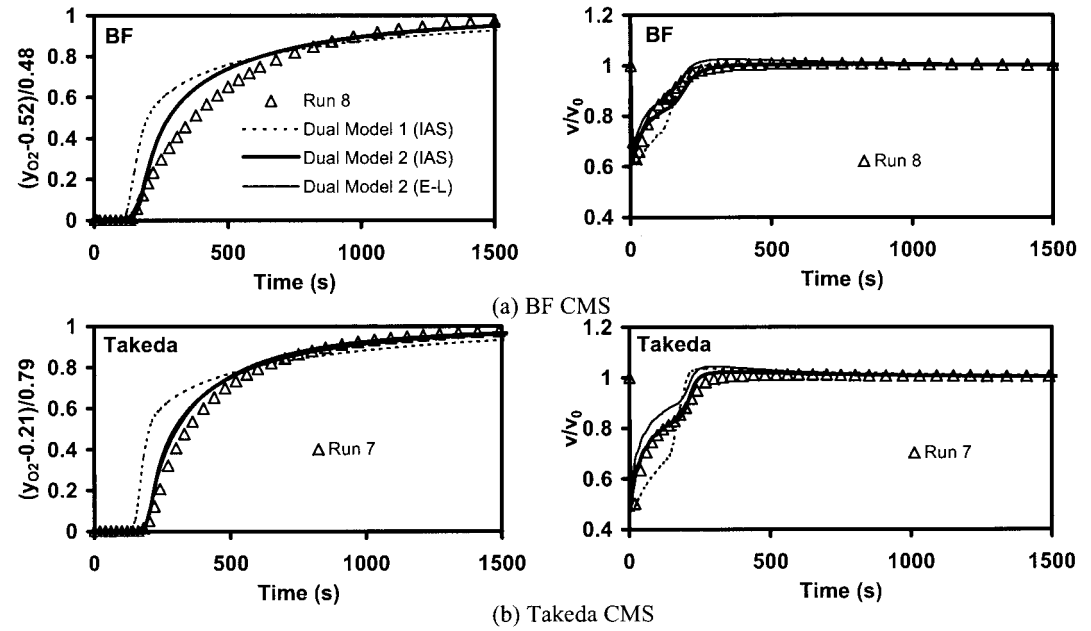

Figure 8. Exit concentration and velocity profiles measured in (a) BF CMS and (b) Takeda CMS beds that were initially saturated with oxygen–nitrogen mixture and then purged with oxygen are compared with model predictions.

Experimental details are given in Table 6.

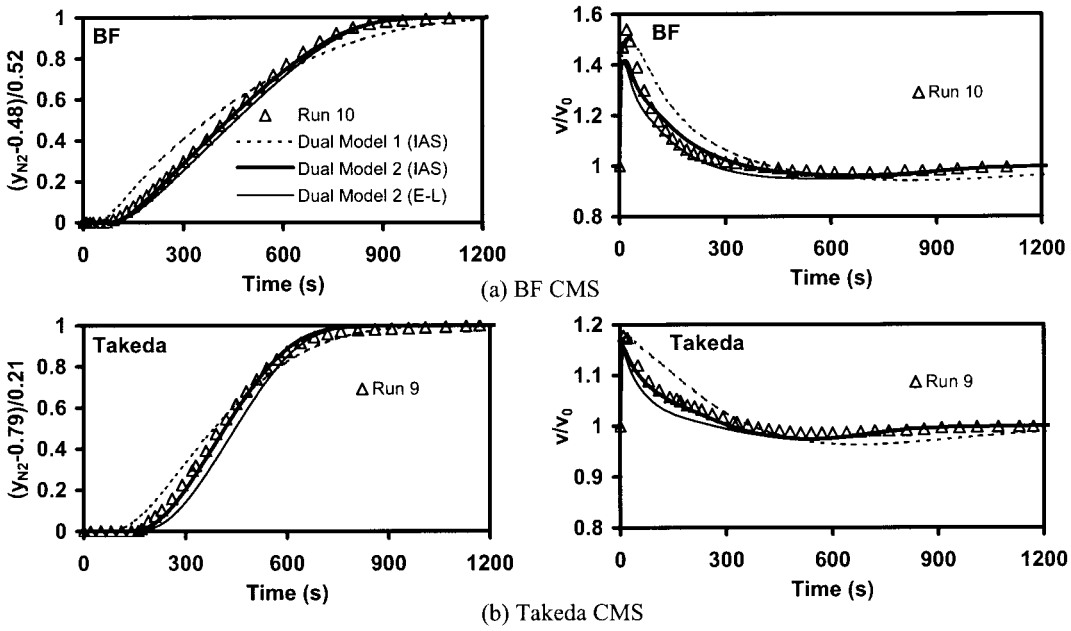

Figure 9. Exit concentration and velocity profiles measured in (a) BF CMS and (b) Takeda CMS beds that were initially saturated with oxygen–nitrogen mixture and then purged with nitrogen are compared with model predictions.

Experimental details are given in Table 6.

mixture and its prediction from Dual Model 2 (see Figure 8). It appears that the actual oxygen uptake was somewhat faster than what the model predicts.

Conclusions

Significant superiority of the dual-resistance model over pore and barrier models for gas transport in the micropores of carbon molecular sieves has been demonstrated by comparing the optimum fits of all models with the measured uptakes of oxygen and nitrogen in BF and Takeda samples at low pressure. Presence of dual-transport resistance in the micropores of these adsorbents has been further validated with single-component breakthrough experiments conducted in the linear range. It has been demonstrated with several single-component and binary experiments that the chemical potential gradient, as the driving force for micropore diffusion with pore-size independent-constant limiting transport parameters completely fails to predict the dynamic responses due to large, step changes in concentration. The thermodynamically corrected transport parameters generally show strong dependence on the adsorbed phase concentration. These results reinforce our similar conclusions in a previous study (Huang et al., 2003). With the proposed empirical equations (Eqs. 8 and 9) to account for the pore-size dependence of the limiting transport parameters, the dual model is able to adequately predict the experimental results. Both extended Langmuir isotherm and IAS theory give satisfactory results for binary calculations. However, the predictions are slightly more accurate with the IAS theory.

The quantitative agreement between model predictions and experimental results is truly remarkable given that all the equilibrium and kinetic parameters are obtained from independent single-component measurements at the particle scale. Although the stronger concentration dependence has been empirically accounted for in the theoretical model, we are not aware of any other model that is able to give good quantitative prediction of binary transport of gases in CMS micropores at high pressure. Our preliminary results for binary and ternary mixtures of other gases are promising and will be reported in a future communication.

Notation

A = surface area per unit mass of adsorbent, cm^2
b = Langmuir constant, cc/mmol
b_o = preexponential constant for temperature dependence of b, cc/mmol
c = gas-phase concentration, mmol/cc
c_e = exit gas concentration, mmol/cc
c_o = constant feed concentration in column dynamic and DAB measurements, mmol/cc
c_p = gas concentration in the macropores, mmol/cc
c_T = total concentration in the gas phase, mmol/cc
c^{im} = imaginary gas-phase concentration in the micropore, mmol/cc
d_p = particle diameter
D_c = micropore diffusivity, cm^2/s
D_{co} = limiting micropore diffusivity, cm^2/s
D^*_{co} = limiting micropore diffusivity in the smallest accessible pore (see Eq. 6), cm^2/s
D'_{co} = preexponential constant for temperature dependence of diffusivity, cm^2/s
D_L = axial dispersion coefficient, cm^2/s
D_m = molecular diffusivity, cm^2/s
D_p = macropore diffusivity, cm^2/s
E_b = activation energy for diffusion across the barrier resistance at the pore mouth, kcal/mol
E_d = activation energy for diffusion in micropore interior, kcal/mol
J = diffusion flux, $mol \cdot cm^{-2} \cdot s^{-1}$
k_f = external fluid mass-transfer coefficient, cm/s
K_c = Henry's constant
k_b = barrier coefficient, s^{-1}

k_{bo} = limiting barrier coefficient, s^{-1}
k^*_{bo} = limiting barrier coefficient at the smallest accessible pore mouth (see Eq. 7), s^{-1}
k'_{bo} = preexponential constant for temperature dependence of barrier coefficient, s^{-1}
L = column length, cm
n = total number of moles of adsorbate adsorbed by adsorbent, mol
N = number of components
P = pressure, bar
P_b = final pressure in desorption system in DAB blank measurement, bar
P_d = final pressure in desorption system in DAB integral uptake measurement, bar
P_i = partial pressure of component i, bar
P^o_i = hypothetical pressure in the IAS theory that yields the same spreading pressure for every component i in the mixture, bar
P_{sys} = pressure in the desorption system, bar
q = adsorbed gas-phase concentration, mmol/cc
q_p = adsorbed gas-phase concentration based on particle volume, mmol/cc
q_s = monolayer saturation capacity according to the Langmuir model, mmol/cc
q_T = total adsorbed amount defined by Eq. 21, mmol/cc
q^o = equilibrium adsorbed amount at pressure P^o, mmol/cc
q^* = equilibrium adsorbed amount based on microparticle volume, mmol/cc
q^*_p = equilibrium adsorbed amount based on macroparticle volume, mmol/cc
$\bar{q}$ = average adsorbate concentration in the micropore, mmol/cc
r = radial distance coordinate of the microparticle, cm
r_c = microparticle radius, cm
R = radial distance coordinate of adsorbent pellet, cm
Re = Reynolds number ($2R_p u\rho/\mu$)
R_g = universal gas constant (=1.987 cal mol^{-1} K^{-1} = 83.14 cc bar mol^{-1} K^{-1})
R_p = adsorbent pellet radius, cm
Sc = Schmidt number ($\mu/\rho D_m$)
Sh = Sherwood number ($2R_p k_f/D_m$)
t = time, s
T = temperature, K
T_{sys} = temperature of desorption system, K
u = superficial velocity in a packed bed, cm/s
ΔU = change of internal energy due to adsorption, kcal/mol
V_d = volume of desorption system, cc
$v(v_o, v_e)$ = interstitial gas velocity (at inlet, at exit) cm/s
x = mole fraction in adsorbed phase
$y(y_o, y_e)$ = mole fraction in gas phase (at inlet, at exit)
y_b = mole fraction of adsorbate in the desorption system in DAB blank measurements
y_d = mole fraction of adsorbate in the desorption system in DAB uptake measurements
z = axial distance along the column length, cm
$0(0^+, 0^-)$ = column inlet (just inside, just outside)

Greek letters

α = parameter defined in the Appendix ($=e^{\Pi/q_s}$)
β_p, β_b = fitting parameters in the proposed empirical models defined by Eqs. 6 and 7
λ = fitting parameter in Eq. 3
μ = gas viscosity, gm · cm^{-1} · s^{-1}
π = spreading pressure, bar
Π = constant defined in Eq. 18
ρ = gas density, gm/cc
τ = mean residence time, s
τ_b = mean residence time of the corresponding blank run, s
ε_b = bed void fraction
ε_p = particle void fraction
θ = fractional coverage of the adsorption sites ($=q/q_s$)
θ^* = fractional coverage of the adsorption sites corresponding to q^* ($=q^*/q_s$)
ζ = dimensionless parameters along the radius of macropore ($=R/R_P$)
η = dimensionless parameters along the radius of micropore ($=r/r_c$)

Subscript

i = ith component (A and B for a binary system)

Literature Cited

Carlson, N. W., and J. S. Dranoff, "Competitive Adsorption of Methane and Ethane on 4A Zeolite," *Fundamentals of Adsorption,* A. L. Liapis, ed., Engineering Foundation, New York (1987).

Chagger, H. K., F. E. N. M. Sykes, and K. M. Thomas, "Kinetic of Adsorption and Diffusional Characteristics of Carbon Molecular Sieves," *Carbon,* **33,** 1405 (1995).

Chen, Y. D., and R. T. Yang, "Predicting Binary Fickian Diffusivities from Pure Component Fickian Diffusivities for Surface Diffusion," *Chem. Eng. Sci.,* **47,** 3895 (1992).

Chen, Y. D., R. T. Yang, and P. Uawithya, "Diffusion of Oxygen, Nitrogen and Their Mixtures in Carbon Molecular Sieve," *AIChE J.,* **44,** 577 (1994).

Chihara, K., M. Suzuki, and K. Kawazoe, "Concentration Dependence of Micropore Diffusivities-Diffusion of Propylene in Molecular Sieving Carbon 5A," *J. Chem. Eng. Jpn.,* **11,** 153 (1978).

Do, D. D., *Adsorption Analysis: Equilibrium and Kinetics,* Imperial College Press, London (1998).

Do, D. D., X. Hu, and P. L. J. Mayfield, "Multicomponent Adsorption of Ethane, *n*-Butane and *n*-Pentane in Activated Carbon," *Gas Sep. Purif.,* **5,** 35 (1991).

Dominguez, J. A., D. Psaras, and A. I. LaCava, "Langmuir Kinetics as an Accurate Simulation of the Rate of Adsorption of Oxygen and Nitrogen Mixtures on Non-Fickian Carbon Molecular Sieves," *AIChE Symp. Ser.,* **84,** 73 (1988).

Farooq, S., Q. L. Huang, and I. A. Karimi, "Identification of Transport Mechanism in Adsorbent Micropores from Column Dynamics," *Ind. Eng. Chem. Res.,* **41,** 1098 (2002).

Farooq, S., and D. M. Ruthven, "Numerical Simulation of a Kinetically Controlled Pressure Swing Adsorption Bulk Separation Process Based on a Diffusion Model," *Chem. Eng. Sci.,* **46,** 2213 (1991).

Fitch, F. R., M. Bulow, and A. I. LaCava, "Investigation of the Mechanism for the Separation of Nitrogen-Oxygen Mixtures on Carbon Molecular Sieves," *Gas Sep. Purif.,* **8,** 45 (1994).

Habgood, H. W., "The Kinetics of Molecular Sieve Action Sorption of Nitrogen, Methane Mixtures by Linde Molecular Sieve 4A," *Can. J. Chem.,* **36,** 1384 (1958).

Hu, X., and D. D. Do, "Multicomponent Adsorption Kinetics of Hydrocarbons onto Activated Carbon," *Chem. Eng. Sci.,* **48,** 1317 (1993).

Huang, Q. L., S. M. Sundaram, and S. Farooq, "Revisiting Transport of Gases in the Micropores of Carbon Molecular Sieves," *Langmuir,* **19,** 393 (2003).

Huang, Q. L., "Multicomponent Diffusion of Gases in the Micropores of Carbon Molecular Sieves," PhD Thesis, National Univ. of Singapore, Singapore (2002).

Kawazoe, K., M. Suzuki, and K. Chihara, "Chromatographic Study of Diffusion in Molecular-Sieving Carbon," *J. Chem. Eng. Jpn.,* **7,** 151 (1974).

LaCava, A. I., V. A. Koss, and D. Wickens, "Non-Fickian Adsorption Rate Behaviour of Some Carbon Molecular Sieves," *Gas Sep. Purif.,* **3,** 180 (1989).

Liu, H., and D. M. Ruthven, "Diffusion in Carbon Molecular Sieves," *Proc. Int. Conf. Fundam. Adsorp.,* M. D. LaVan, ed., Kluwar Press, Boston (1996).

Loughlin, K. F., M. M. Hassan, A. I. Fatehi, and M. Zahur, "Rate and Equilibrium Sorption Parameters for Nitrogen and Methane on Carbon Molecular Sieve," *Gas Sep. Purif.,* **7,** 264 (1993).

Malek, A., "A Study of Hydrogen Purification from the Refinery Fuel Gas by Pressure Swing Adsorption," PhD Thesis, National Univ. of Singapore, Singapore (1996).

Malek, A., and S. Farooq, "Determination of Equilibrium Isotherms Using Dynamic Column Breakthrough and Constant Flow Equilibrium Desorption," *J. Chem. Eng. Data,* **41,** 25 (1996).

Malek, A., and S. Farooq, "Kinetics of Hydrocarbon Adsorption on Activated Carbon and Silica Gel," *AIChE J.,* **43,** 761 (1997).

Myers, A. L., and J. M. Prausnitz, "Thermodynamics of Mixed-Gas Adsorption," *AIChE J.,* **11,** 121 (1965).

Nguyen, C., and D. D. Do, "Dual Langmuir Kinetic Model for Adsorption in Carbon Molecular Sieve Materials," *Langmuir,* **16,** 1868 (2000).
Rao, M. B., and S. Sircar, "Thermodynamic Consistency For Binary Gas Adsorption Equilibria," *Langmuir,* **15,** 7258 (1999).
Reid, C. R., I. P. O'koye, and K. M. Thomas, "Adsorption of Gases on Carbon Molecular Sieves Used for Air Separation. Spherical Adsorptives as Probes for Kinetic Selectivity," *Langmuir,* **14,** 2415 (1998).
Reid, C. R., and K. M. Thomas, "Adsorption of Gases on a Carbon Molecular Sieves Used for Air Separation: Linear Adsorptives as Probes for Kinetic Selectivity," *Langmuir,* **15,** 3206 (1999).
Reid, C. R., and K. M. Thomas, "Adsorption Kinetics and Size Exclusion Properties of Probe Molecules for the Selective Porosity in a Carbon Molecular Sieve Used for Air Separation," *J. Phys. Chem. B,* **105,** 10619 (2001).
Rutherford, S. W., and D. D. Do, "Adsorption Dynamics of Carbon Dioxide on a Carbon Molecular Sieve 5A," *Carbon,* **38,** 1339 (2000).
Ruthven, D. M., *Principles of Adsorption and Adsorption Processes,* Wiley, New York (1984).
Ruthven, D. M., "Diffusion of Nitrogen and Oxygen in Carbon Molecular Sieve," *Chem. Eng. Sci.,* **47,** 4305 (1992).
Ruthven, D. M., N. S. Ragavan, and M. M. Hassan, "Adsorption and Diffusion of Nitrogen and Oxygen in a Carbon Molecular Sieve," *Chem. Eng. Sci.,* **41,** 1325 (1986).
Rynders, R. M., M. B. Rao, and S. Sircar, "Isotope Exchange Technique for Measurement of Gas Adsorption Equilibria and Kinetics," *AIChE J.,* **43,** 2456 (1997).
Sherwood, T. K., R. L. Pigford, and C. R. Wilke, *Mass Transfer,* McGraw-Hill, New York (1975).
Srinivasan, R., S. R. Auvil, and J. M. Schork, "Mass Transfer in Carbon Molecular Sieves—An Interpretation of Langmuir Kinetics," *Chem. Eng. J.,* **57,** 137 (1995).
Van den Broeke, L. J. P., and R. Krishna, "Experimental Verification of the Maxwell-Stefan Theory for Micropore Diffusion," *Chem. Eng. Sci.,* **50,** 2507 (1995).
Wakao, N., and T. Funarzkri, "Effect of Fluid Dispersion Coefficient on Particle-to-Fluid Mass Transfer Coefficients in Packed Beds," *Chem. Eng. Sci.,* **33,** 1375 (1978).
Wang, K., H. Suda, and K. Haraya, "Permeation Time Lag and the Concentration Dependence of the Diffusion Coefficient of CO_2 in a Carbon Molecular Sieve Membrane," *Ind. Eng. Chem. Res.,* **40,** 2942 (2001).
Yuan, Y. X., "Adsorption and Diffusion of Oxygen and Nitrogen in a Carbon Molecular Sieve," Master's Thesis, National Univ. of Singapore, Singapore (1996).

Appendix

For convenience, the boundary conditions for micropore mass balance at $r = r_c$ in Eq. 36 was rewritten as:

$$\frac{3(D_{co})_i}{r_c}\frac{dc_i^{im}}{dr}\bigg|_{r=r_c} = (k_{bo})_i\frac{dc_i^{im}}{dq_i}(q_i^* - q_i)|_{r=r_c}. \tag{A1}$$

When IAS theory is used in the binary calculations, c_A^{im} and c_B^{im} in the micropores are functions of both q_A and q_B and their differentials can be expressed as:

$$\left.\begin{aligned} dc_A^{im} &= \frac{\partial c_A^{im}}{\partial q_A}dq_A + \frac{\partial c_A^{im}}{\partial q_B}dq_B \\ dc_B^{im} &= \frac{\partial c_B^{im}}{\partial q_A}dq_A + \frac{\partial c_B^{im}}{\partial q_B}dq_B \end{aligned}\right\}. \tag{A2}$$

Therefore, (dc_A^{im}/dq_A) and (dc_B^{im}/dq_B) in Eq. A1 are

$$\left.\begin{aligned} \frac{dc_A^{im}}{dq_A} &= \frac{\partial c_A^{im}}{\partial q_A} + \frac{\partial c_A^{im}}{\partial q_B}\frac{dq_B}{dq_A} = \frac{\partial c_A^{im}}{\partial q_A} + \frac{\partial c_A^{im}}{\partial q_B}\frac{q_B^* - q_B}{q_A^* - q_A} \\ \frac{dc_B^{im}}{dq_B} &= \frac{\partial c_B^{im}}{\partial q_A}\frac{dq_A}{dq_B} + \frac{\partial c_B^{im}}{\partial q_B} = \frac{\partial c_B^{im}}{\partial q_A}\frac{q_A^* - q_A}{q_B^* - q_B} + \frac{\partial c_B^{im}}{\partial q_B} \end{aligned}\right\} \tag{A3}$$

From Eq. 18, we have

$$\left.\begin{aligned} c_A^o &= \frac{P_A^o}{R_gT} = \frac{\alpha_A - 1}{b_A} \\ c_B^o &= \frac{P_B^o}{R_gT} = \frac{\alpha_B - 1}{b_B} \end{aligned}\right\}, \tag{A4}$$

where $\alpha_A = e^{\Pi/q_{sA}}$ and $\alpha_B = e^{\Pi/q_{sB}}$. Note that $\alpha_B = \alpha_A^{q_{sA}/q_{sB}}$.

Substituting Eq. A4 into Eq. 22, we obtain:

$$\left.\begin{aligned} q_A^o &= \frac{q_{sA}(\alpha_A - 1)}{\alpha_A} \\ q_B^o &= \frac{q_{sB}(\alpha_B - 1)}{\alpha_B} \end{aligned}\right\}. \tag{A5}$$

We combine Eqs. A5, 21, and 23 to get the following equation:

$$\frac{q_A\alpha_A}{q_{sA}(\alpha_A - 1)} + \frac{q_B\alpha_B}{q_{sB}(\alpha_B - 1)} = 1. \tag{A6}$$

In the preceding equation, q_A and q_B are known in the micropores. Π in α_A and α_B is the only unknown that can be solved using the nonlinear equation solver subroutine NEQNF.

Substituting Eq. A4 into Eq. 16, and then combining with Eqs. 19 and 23, one obtains:

$$\left.\begin{aligned} c_A^{im} &= \frac{Py_A}{R_gT} = \frac{q_A(\alpha_A - 1)}{b_A(q_A + q_B)} \\ c_B^{im} &= \frac{Py_B}{R_gT} = \frac{q_B(\alpha_B - 1)}{b_B(q_A + q_B)} \end{aligned}\right\}. \tag{A7}$$

Therefore, we have:

$$\left.\begin{aligned} \frac{\partial c_A^{im}}{\partial q_A} &= \frac{\alpha_A - 1}{b_A(q_A + q_B)}\left(\frac{q_A}{\alpha_A - 1}\frac{\partial \alpha_A}{\partial q_A} + \frac{q_B}{q_A + q_B}\right) \\ \frac{\partial c_A^{im}}{\partial q_B} &= \frac{\alpha_A - 1}{b_A(q_A + q_B)}\left(\frac{q_A}{\alpha_A - 1}\frac{\partial \alpha_A}{\partial q_B} - \frac{q_A}{q_A + q_B}\right) \\ \frac{\partial c_B^{im}}{\partial q_A} &= \frac{\alpha_B - 1}{b_B(q_A + q_B)}\left(\frac{q_B}{\alpha_B - 1}\frac{\partial \alpha_B}{\partial q_A} - \frac{q_B}{q_A + q_B}\right) \\ \frac{\partial c_B^{im}}{\partial q_B} &= \frac{\alpha_B - 1}{b_B(q_A + q_B)}\left(\frac{q_B}{\alpha_B - 1}\frac{\partial \alpha_B}{\partial q_B} + \frac{q_A}{q_A + q_B}\right) \end{aligned}\right\}. \tag{A8}$$

From Eq. A6, expressions for $(\partial\alpha_A/\partial q_A)$, $(\partial\alpha_A/\partial q_B)$, $(\partial\alpha_B/\partial q_A)$, and $(\partial\alpha_B/\partial q_B)$ are obtained:

$$\left.\begin{aligned}
\frac{\partial\alpha_A}{\partial q_A} &= \left[\frac{q_A}{\alpha_A(\alpha_A-1)} + \left(\frac{q_{sA}}{q_{sB}}\right)^2 \frac{q_B\alpha_B(\alpha_A-1)}{\alpha_A^2(\alpha_B-1)^2}\right]^{-1} \\
\frac{\partial\alpha_A}{\partial q_B} &= \left[\frac{q_A(\alpha_B-1)}{\alpha_B(\alpha_A-1)^2}\frac{q_{sB}}{q_{sA}} + \frac{q_{sA}}{q_{sB}}\frac{q_B}{\alpha_A(\alpha_B-1)}\right]^{-1} \\
\frac{\partial\alpha_B}{\partial q_A} &= \left[\frac{q_A}{\alpha_B(\alpha_A-1)}\frac{q_{sB}}{q_{sA}} + \frac{q_{sA}}{q_{sB}}\frac{q_B(\alpha_A-1)}{\alpha_A(\alpha_B-1)^2}\right]^{-1} \\
\frac{\partial\alpha_B}{\partial q_B} &= \left[\frac{q_A\alpha_A(\alpha_B-1)}{\alpha_B^2(\alpha_A-1)^2}\left(\frac{q_{sB}}{q_{sA}}\right)^2 + \frac{q_B}{\alpha_B(\alpha_B-1)}\right]^{-1}
\end{aligned}\right\}. \quad \text{(A9)}$$

Substituting Eq. A3 into Eq. A1, the following equations are obtained:

$$\left.\begin{aligned}
&\frac{3(D_{co})_A}{r_c}\frac{dc_A^{im}}{dr}\bigg|_{r=r_c} \\
&\quad = (k_{bo})_A\left[\frac{\partial c_A^{im}}{\partial q_A}(q_A^* - q_A) + \frac{\partial c_A^{im}}{\partial q_B}(q_B^* - q_B)\right]\bigg|_{r=r_c} \\
&\frac{3(D_{co})_B}{r_c}\frac{dc_B^{im}}{dr}\bigg|_{r=r_c} \\
&\quad = (k_{bo})_B\left[\frac{\partial c_B^{im}}{\partial q_A}(q_A^* - q_A) + \frac{\partial c_B^{im}}{\partial q_B}(q_B^* - q_B)\right]\bigg|_{r=r_c}
\end{aligned}\right\}, \quad \text{(A10)}$$

where $(\partial c_A^{im}/\partial q_A)$, $(\partial c_A^{im}/\partial q_B)$, $(\partial c_B^{im}/\partial q_A)$, and $(\partial c_B^{im}/\partial q_B)$ are obtained by using Eq. A8 in Eq. A9.

Manuscript received Nov. 6, 2002, and revision received June 14, 2003.